JTTEE5 19:551–557
DOI: 10.1007/s11666-009-9462-7
1059-9630/$19.00 © ASM International

Effect of NiCr Clad BaF_2·CaF_2 Addition on Wear Performance of Plasma Sprayed Chromium Carbide-Nichrome Coating

Lingzhong Du, Chuanbing Huang, Weigang Zhang, Jingmin Zhang, and Wei Liu

(Submitted March 31, 2009; in revised form October 19, 2009)

NiCr clad BaF_2·CaF_2 fluoride eutectic powders were added into chromium carbide-nichrome feedstock to improve the tribological properties of NiCr-Cr_3C_2 coating, and the structures, mechanical, and ball-on-disk sliding wear performance of the coating were characterized. The results show that NiCr cladding can effectively decrease the density and thermophysical difference between the feedstock components, while alleviate the decarburization and oxidization of the constituent phases, and form the coating with a uniform and dense microstructure. However, the addition of BaF_2·CaF_2 has a negative effect on mechanical properties of the coating. When the temperature reaches 500 °C, the BaF_2·CaF_2 eutectic is soften by the heat and smeared by the counterpart, thus the low shear stress lubricating film forms between the contact surface, that improves the tribological properties dramatically. At this temperature, the dominant wear mechanisms also change from splats spallation and abrasive wear at room temperature to plastic deformation and plawing by the counterpart. Within the temperature range from 600 to 800 °C, the friction coefficient, the wear rates of NiCr/Cr_3C_2-10% BaF_2·CaF_2 coating and its coupled Si_3N_4 ball are 20%, 40%, and 75% lower than those of the NiCr/Cr_3C_2 coating, respectively. The NiCr/Cr_3C_2-BaF_2·CaF_2 coating shows superior wear performance to the NiCr/Cr_3C_2 coating without lubricant additive.

Keywords metal-matrix composite, solid lubricant coating, sliding wear, thermal spray coating, wear testing

1. Introduction

Thermal sprayed chromium carbide-nichrome coatings are generally produced for wear applications at the elevated temperature involving sliding, fretting, abrasion, and erosion in energy conversion and utilization systems like steam turbines, gas turbines, etc. (Ref 1-9). However, the high friction coefficient always leads the severe wear of the couple parts. BaF_2·CaF_2 fluoride eutectic with a much lower melting point (1050 °C) than BaF_2 (1338 °C) and CaF_2 (1410 °C) and with lower shear stress shows good lubrication under the temperature ranging between 400 and 900 °C and has been blended with NiCr and Cr_3C_2 powder to improve the wear properties of thermal sprayed NiCr-Cr_3C_2 coating (Ref 10, 11). However, the feedstock material prepared by a simple mechanically mixed NiCr, Cr_3C_2, and BaF_2·CaF_2 components has many serious disadvantages. Different density and thermophysical properties of each constituent phase usually lead to separate trajectories and poor microstructure in the final coating. Also, the oxidation and decarburization of Cr_3C_2 powders during thermal spray result in poor wear resistance of the coating (Ref 12). In this study, a new feedstock preparation method by blending NiCr-coated BaF_2·CaF_2 fluoride eutectic and NiCr-coated Cr_3C_2 powders is used to overcome the shortcomings mentioned above, and the effect of the BaF_2·CaF_2 eutectic addition on the mechanical and wear performance of the plasma sprayed chromium carbide coatings is also investigated.

Lingzhong Du, Chuanbing Huang, Weigang Zhang, and **Wei Liu**, State Key Laboratory of Multi-Phase Complex System, Institute of Process Engineering, Chinese Academy of Sciences, Beijing 100080, P.R. China; and **Jingmin Zhang**, China Iron & Steel Research Institute Group, Beijing 100081, P.R. China. Contact e-mail: dulingzhong@hotmail.com.

2. Materials and Experimental Procedures

2.1 Preparation of Feedstock and Coatings

Ni-coated Cr_3C_2 (Ni/Cr_3C_2) and Ni-coated BaF_2·CaF_2 (62:38 wt.%) eutectic (Ni/BaF_2·CaF_2) powders were, respectively, manufactured by the process of hydrothermal hydrogen reduction, as follows:

$$\mathrm{Ni(NH_3)_nSO_4 + H_2 + Cr_3C_2 \xrightarrow{surfactant} Ni/Cr_3C_2 + (NH_4)_2SO_4 + (n-2)NH_3 \quad (n \geq 2)}$$

$$\mathrm{Ni(NH_3)_nSO_4 + H_2 + eutectic \xrightarrow{surfactant} Ni/eutectic + (NH_4)_2SO_4 + (n-2)NH_3 \quad (n \geq 2)}$$

In the above reaction, the metallic nickel was reduced onto core particles from ammoniacal solution by hydrogen

under pressure at a temperature of 150 °C in autoclaves. Then, the Ni/Cr_3C_2 and Ni/BaF_2·CaF_2 were, respectively, chromized to form NiCr-coated composite powders (NiCr/Cr_3C_2 and NiCr/BaF_2·CaF_2). The feedstocks with the required lubricant content were prepared by blending the NiCr/Cr_3C_2 (Ni:Cr:Cr_3C_2 = 20:5:75, wt.%) and NiCr/BaF_2·CaF_2 (Ni:Cr:BaF_2·CaF_2 = 40:10:50, wt.%) powders at the calculated ratio, as summarized in Table 1. The NiCr clad Cr_3C_2 powders without added lubricants functioned as the control or baseline coating to which the modified coatings were compared.

Before coating preparation, inconel X-750 superalloy substrates with a size of 30 × 40 mm^2 were grit blasted with coarse Al_2O_3 particles (about 600 μm) to roughen the surface, and then deposited NiAl for bond coating to improve the adhesion of the coating. The bond and top coatings were deposited by a commercial APS2000 K plasma spray system (Aeronautical Manufacturing Technology Research Institute, China) at optimal spray parameters, as summarized in Table 2. The thickness of NiAl bond coat and top composite layer was around 0.1 and 0.5 mm, respectively.

2.2 Coating Characterization

Vickers microhardness indentations (Shanghai Taiming Optical, China) with a load of 1.96 N and a dwell time of 15 s were made onto the polished cross section of the as-sprayed coatings to avoid the influence of the substrate. The microhardness of the coatings represented average of 10 indentations. Bond strength of the as-sprayed coatings was evaluated using a pull-off adhesion bond method as ASTM standard C-633. The crystal phases were characterized by an X'Pert Pro X-ray diffraction meter (Panalytical, Netherlands) with a Cu Kα radiation.

2.3 Tribological Test

Friction and wear tests were conducted by HT-1000 "ball-on-disk" high temperature wear test equipment (Lanzhou Institute of Chemical Physics, China) under dry sliding condition in the air. The lower disk specimen of inconel X-750 superalloy was rotating, with a dimension of ∅25 × 5 mm^2. The thickness of composite coating deposited onto the superalloy disk was about 0.5 mm after grinding and polishing. The mating upper sintered Si_3N_4 ceramic ball (Shanghai Research Institute of Materials, China) was stationary, with a diameter of ∅ = 6 mm. Before the test, the disk and Si_3N_4 ceramic ball were cleaned by acetone and ultrasonic. The wear couples were surrounded by an electric resistance furnace and heated to the pre-set test temperature at a rate of 10 K/min. The temperature deviation was controlled to be within ±2 K. All tests were commenced at a load of 10 N with a sliding diameter of 10 mm and a sliding velocity of 0.188 m/s for duration of 20 min. The friction coefficient was recorded during each test and the mean values were calculated.

The cross section area of the worn track was measured using Talysurf 5P-120 surface profilometer (Rank Taylor Hobson, UK), and the area was multiplied by the track circumference to determine the disk wear volume. The wear volume of the counterpart was calculated by measuring the circular wear scar on the ball surface. The specific wear rates were obtained by dividing the wear volume by the load and the total sliding distance. To insure the reproducibility of the measurements, three repeated tests were executed under the same test conditions. The microstructures were investigated by scanning electron microscope (SEM), as well as chemical qualitative and semiquantitative analysis by energy-dispersive spectrometer (EDS).

Table 1 Blended ratio of NiCr/Cr_3C_2 and NiCr/BaF_2·CaF_2 powders in the feedstock

25NiCr/75Cr_3C_2 ratio, wt.%	50NiCr/50BaF_2·CaF_2 ratio, wt.%	BaF_2·CaF_2, wt.%
100	0	0
90	10	5
80	20	10
70	30	15
60	40	20

3. Results and Discussion

3.1 Microstructure

The SEM image in Fig. 1(a) shows that the composite powders consist of blended NiCr/Cr_3C_2 (80 wt.%) and NiCr/BaF_2·CaF_2 (20 wt.%) with angular shape and size distribution between 45 and 75 μm. The cross section of the NiCr/BaF_2·CaF_2 (Fig. 1b) in backscattered electron image reveals that fluoride eutectic has a laminar structure, in which rounded CaF_2 grains (dark region in A) are uniformly distributed in the BaF_2 matrix (bright region in A) as observed by the other researcher (Ref 13). From the images, it is obviously that all of Cr_3C_2 (Fig. 1c) and BaF_2·CaF_2 particles have been completely and densely coated within the NiCr metallic binder. It is expected to

Table 2 Thermal spray parameters

System	Voltage, V	Current, A	Ar pressure, MPa	Ar flow rate, L/min
APS2000K	60	600	0.6	35
H_2 pressure, MPa	**H_2 flow rate, L/min**	**Carrier gas pressure, N_2, MPa**	**Powder feed rate, g/min**	**Spray distance, mm**
0.45	2	0.3	45	90

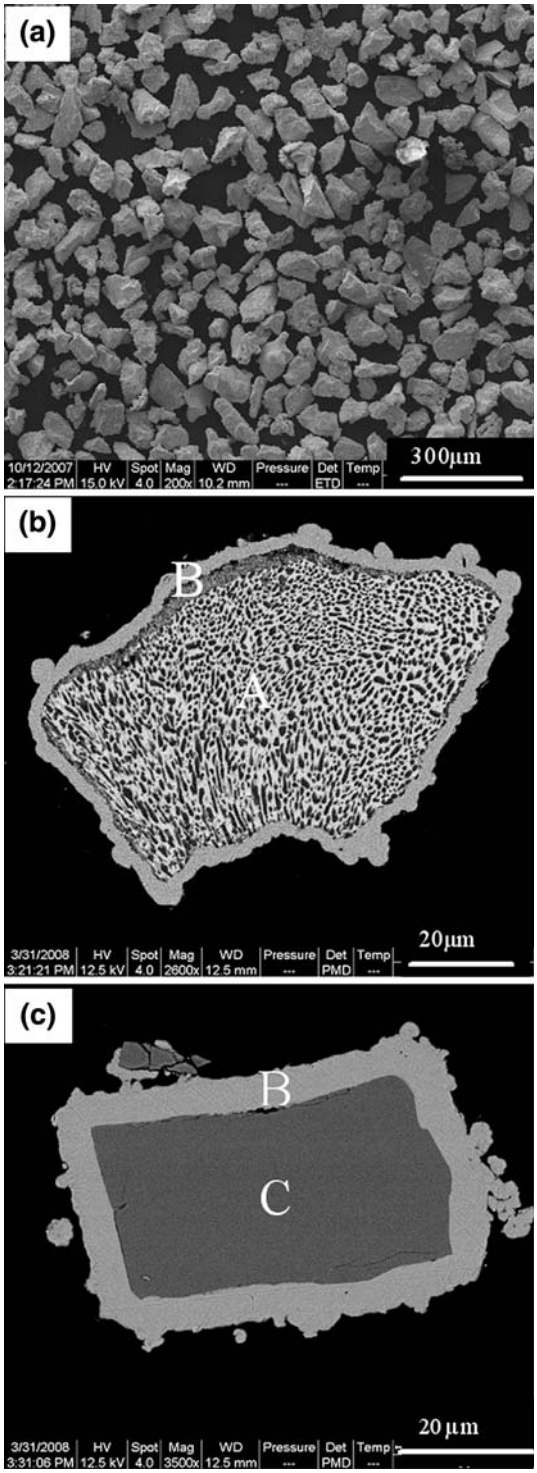

Fig. 1 SEM micrographs of the feedstock (80 wt.% $NiCr/Cr_3C_2$ blended with 20 wt.% $NiCr/BaF_2{\cdot}CaF_2$) (a) blended powder surface, (b) $NiCr/BaF_2{\cdot}CaF_2$ cross section, (c) $NiCr/Cr_3C_2$ cross section. Regions A, B, and C correspond to $BaF_2{\cdot}CaF_2$ eutectic, NiCr alloy, and Cr_3C_2, respectively

prevent decarburization and oxidization of the cores, as well as to produce dense coating by melting of the surrounding binder during the thermal spraying process.

Table 3 Properties of the feedstock

	Flowability, s/50 g	Apparent density, g/cm^3
$50NiCr/50BaF_2{\cdot}CaF_2$	59	1.85
$25NiCr/75Cr_3C_2$	62	1.92

As summarized in Table 3, the $NiCr/BaF_2{\cdot}CaF_2$ powders with 50 wt.% NiCr and $NiCr/Cr_3C_2$ powders with 25 wt.% NiCr have almost the same apparent density and the flowability, which expects to eliminate the negative effect of the separation of the blended feedstock in particle trajectories in the plasma jet.

Cross-sectional SEM images of the as-sprayed coatings with 0%, 10%, and 20% $BaF_2{\cdot}CaF_2$ in the powders are shown in Fig. 2. Relatively dense coatings are well bonded with the substrates and lamellae microstructures elongated in the direction parallel to surface are observed, typically seen in plasma spray coating (Ref 14, 15). The porosity of the coatings estimated by image analysis increases from 3.63%, 4.73% to 5.42% with increase of the $BaF_2{\cdot}CaF_2$ ratio. An EDS examination of the microstructure of the coating with 10% $BaF_2{\cdot}CaF_2$ content in the powders reveals the darkest spot, marked by A in Fig. 4(d), corresponds to the pores. Also, the gray angular field of B, the bright gray area of C, and the broken particles of D correspond to Cr_3C_2, NiCr and $BaF_2{\cdot}CaF_2$ fluoride, respectively.

X-ray diffraction patterns of the starting powder and the as-sprayed coating with 10% $BaF_2{\cdot}CaF_2$ content in the powders are shown in Fig. 3. Before and after the spraying, all peaks of NiCr, Cr_3C_2, BaF_2, and CaF_2 are found in the XRD patterns, and no obvious peaks from Cr_7C_3 and $Cr_{23}C_6$ are detected in the coating. The decarburization of Cr_3C_2 to Cr_7C_3 or $Cr_{23}C_6$ is associated with oxidation of Cr_3C_2 by heating of sprayed particles (Ref 16). It is expected that densely coated NiCr alloy can effectively prevent oxidation, thus the decarburization is lower. It is common knowledge now that low decarburization will markedly improve the wear resistance of the Cr_3C_2 coating.

3.2 Mechanical Properties

The effect of the $BaF_2{\cdot}CaF_2$ eutectic addition on the mechanical properties of the coatings are shown in Fig. 4. The Vickers microhardness in Fig. 4(a) and bond strength in Fig. 4(b) decrease slightly when the content of $BaF_2{\cdot}CaF_2$ eutectic in the powders is $<10\%$. When the $BaF_2{\cdot}CaF_2$ eutectic exceeds 10%, they both drop sharply. It is evident that increase of the $BaF_2{\cdot}CaF_2$ eutectic in the powders has a negative influence on the microhardness and bond strength of the sprayed coatings, which may result from the soft nature of the $BaF_2{\cdot}CaF_2$ eutectic (eutectic $HV_{0.2} = 450$, Cr_3C_2 $HV_{0.2} = 1400$) and poor bond strength of $BaF_2{\cdot}CaF_2$ eutectic when it melt in the plasma flame and broke during colliding on the substrate, as observed in Fig. 4(d).

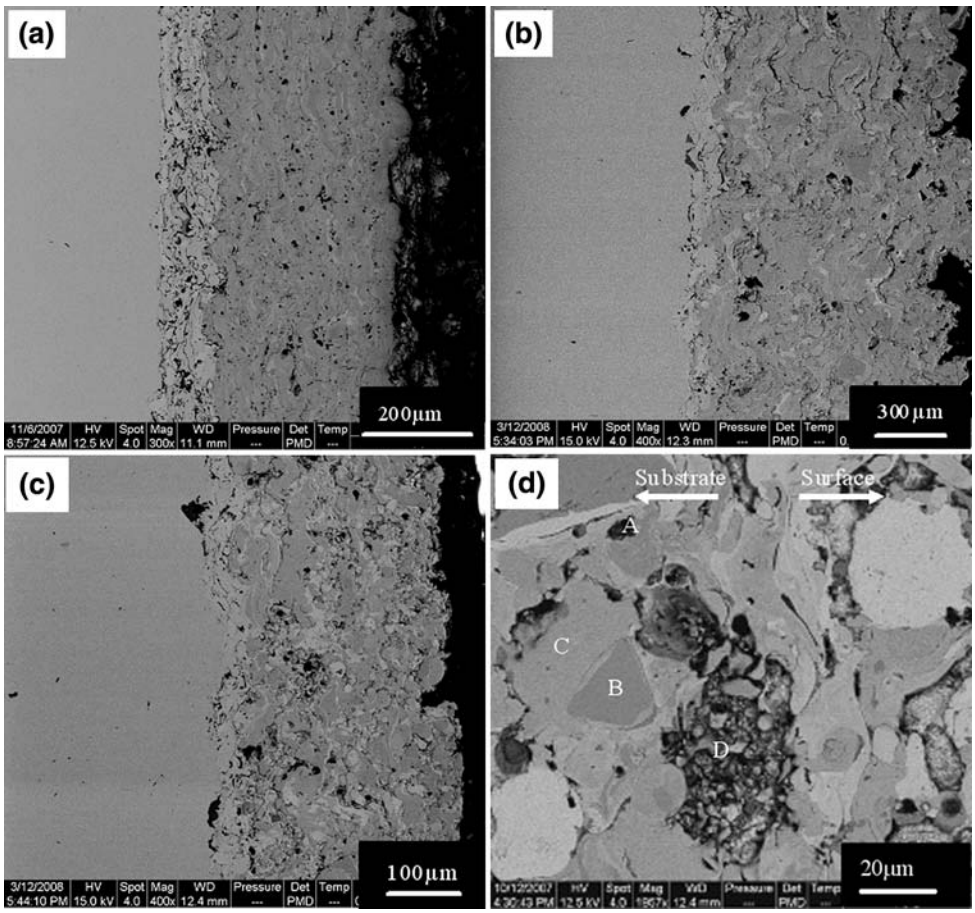

Fig. 2 SEM micrographs of the cross section of the as-sprayed NiCr/Cr_3C_2-BaF_2·CaF_2 coatings, (a) with no BaF_2·CaF_2, (b) with 10% BaF_2·CaF_2, (c) with 20% BaF_2·CaF_2 in the powders, and (d) higher magnification micrograph of (b)

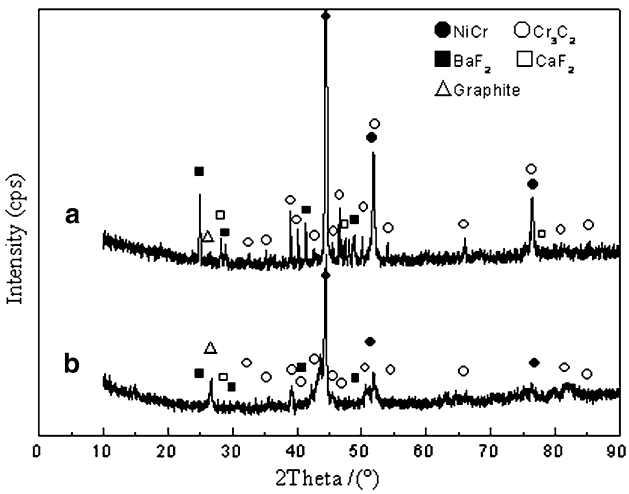

Fig. 3 XRD patterns of the composite NiCr/Cr_3C_2-BaF_2·CaF_2 powder with 10% BaF_2·CaF_2 addition and the as-sprayed coating

As is well known, the microhardness and bond strength are two vital important factors for the wear performance of the coating and too low microhardness and bond strength will lead to the poor wear resistance. Therefore, the coating of 10% BaF_2·CaF_2 eutectic in the powders (defined as NiCr/Cr_3C_2-10%BaF_2·CaF_2) is selected to test its tribological properties.

3.3 Tribological Properties

Typical friction coefficients between wear couples with sliding distance at 600 °C and steady friction coefficients from room temperature to 800 °C of the NiCr/Cr_3C_2 coating and the NiCr/Cr_3C_2-10%BaF_2·CaF_2 coating are shown in Fig. 5. The friction coefficients of both coatings (Fig. 5a) increase gradually with sliding distance due to the running-in at the start of the test, and then decrease to relatively steady value. The friction coefficient and its fluctuations of NiCr/Cr_3C_2-10%BaF_2·CaF_2 coating are lower than those of NiCr/Cr_3C_2 coating. As the temperature increases, the friction coefficients of both NiCr/Cr_3C_2 and NiCr/Cr_3C_2-10%BaF_2·CaF_2 coatings increase below 300 °C, and then decrease. From room temperature to 500 °C, the friction coefficient of the NiCr/Cr_3C_2-10%BaF_2·CaF_2 coating is only about 5% lower than that of NiCr/Cr_3C_2 coating. When the temperature exceeds 500 °C, the friction coefficient of the NiCr/Cr_3C_2-10%BaF_2·CaF_2

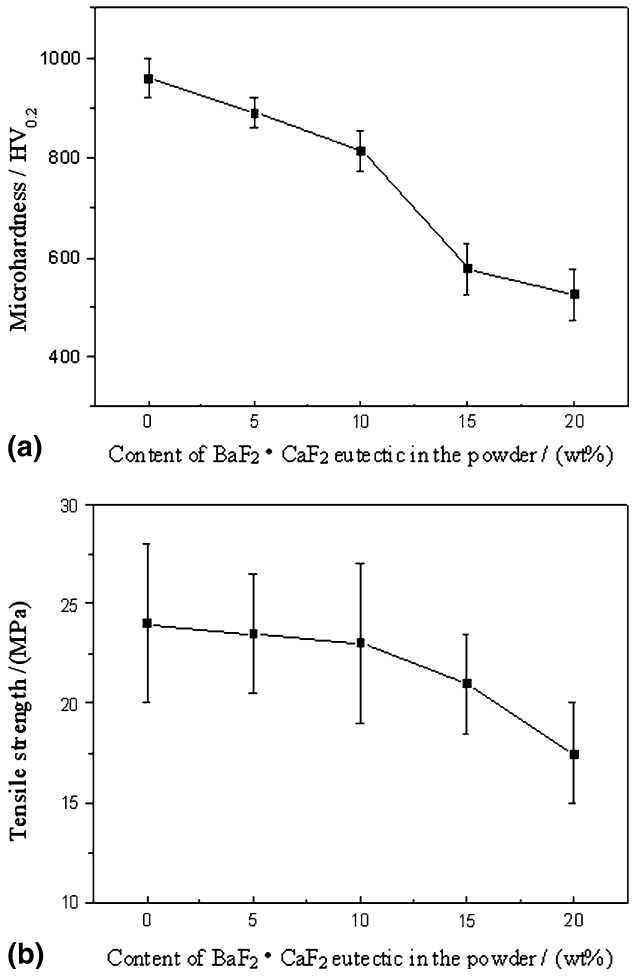

Fig. 4 Microhardness (a) and bond strength (b) of the NiCr/Cr_3C_2-BaF_2·CaF_2 coatings with the content of BaF_2·CaF_2 in the powders

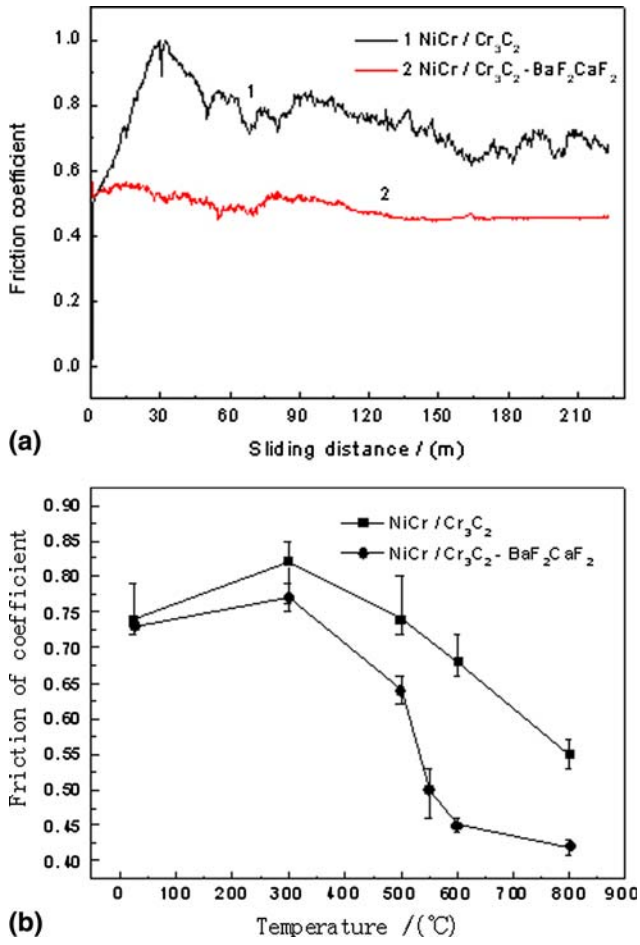

Fig. 5 Typical friction coefficients between wear couples with sliding distance at 600 °C (a) and steady friction coefficients from room temperature to 800 °C (b) of the NiCr/Cr_3C_2 coating and the NiCr/Cr_3C_2-10%BaF_2·CaF_2 coating

coating has a notable reduction. It is about 0.4-0.5, and is 20% lower than that of the NiCr/Cr_3C_2 coating in the temperature region between 500 and 800 °C.

The specific wear rates of the NiCr/Cr_3C_2 coating, the NiCr/Cr_3C_2-10%BaF_2·CaF_2 coating and their counterpart Si_3N_4 balls from room temperature to 800 °C are shown in Fig. 6. Below 500 °C, the wear rates of both NiCr/Cr_3C_2 and NiCr/Cr_3C_2-10%BaF_2·CaF_2 coatings increase with increasing temperature, where the wear rate of the NiCr/Cr_3C_2 coating is lower than that of the NiCr/Cr_3C_2-10%BaF_2·CaF_2 coating. When the temperature exceeds 500 °C, the wear rate of the NiCr/Cr_3C_2 coating changes little, whereas the wear rate of the NiCr/Cr_3C_2-10%BaF_2·CaF_2 coating decreases from 10×10^{-5} to 5×10^{-5} mm^3/N m. In the temperature region between 500 and 800 °C, the wear rate of the NiCr/Cr_3C_2-10%BaF_2·CaF_2 coating exhibits 40% lower than that of the NiCr/Cr_3C_2 coating. From Fig. 6(b), it can be seen that the wear rate of the Si_3N_4 ball for the NiCr/Cr_3C_2 coating increases at first with increasing temperature, and then decreases. On the other hand, the wear rate of the NiCr/Cr_3C_2-10%BaF_2·CaF_2 coating decreases monotonously. At the temperature from 600 to 800 °C, the wear rate of the Si_3N_4 ball for the NiCr/Cr_3C_2-10%BaF_2·CaF_2 coating is 75% lower than that for the NiCr/Cr_3C_2 coating.

Within the study, the tribological properties of NiCr/Cr_3C_2 coating improve by addition of the BaF_2·CaF_2 under the temperature of higher than 500 °C. To investigate the wear mechanism, SEM images of worn surface for the NiCr/Cr_3C_2-10% BaF_2·CaF_2 coating at room temperature and 500 °C are shown in Fig. 7(a) and (b). The worn surface of the coating at room temperature shows a rough surface with tiny wear scars grooved in the wear track. Under the continuous friction force, the splats will fracture and spalled at the weak regions, such as microcracks and pores. The spalled debris then acts as hard particles to plow the coating. Therefore at the room temperature, delamination and abrasive wear are considered to be two dominant wear mechanisms. With the temperature reaching up to 500 °C, the worn surface of the coating

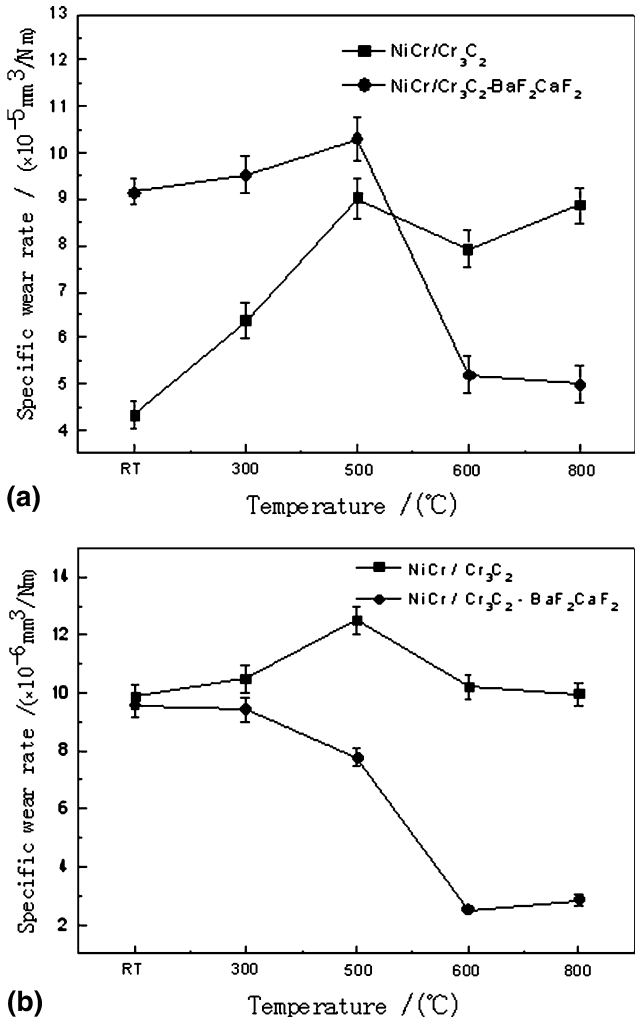

Fig. 6 Specific wear rates with temperature of the $NiCr/Cr_3C_2$ coating and the $NiCr/Cr_3C_2$-10%$BaF_2{\cdot}CaF_2$ coating (a) and their counterpart Si_3N_4 balls (b)

shown in Fig. 7(b) becomes smooth and is covered by a glaze layer. EDS analysis (Fig. 7c) confirms that the layer mainly consists of O, Cr, C, Ba, Ca, and F with a little Si and Ni. It is obvious that a solid lubricous film selectively builds up on the sliding contact surface when the $BaF_2{\cdot}CaF_2$ eutectic is soften at high temperature and smeared by the Si_3N_4 ball. This low shear stress lubricous film could effectively prevent fracture and spallation. At this temperature, the wear loss would be dominated by plastic deformation under pressure contact and then plowing by the counterpart. Based on the results, it is clear that the NiCr cladding can effectively reduce the difference of the density and thermophysical properties between the feedstock component and protect the cores from oxidation and decarburization. $NiCr/Cr_3C_2$ coating of 10% $BaF_2{\cdot}CaF_2$ eutectic in the powders shows low friction coefficient and high wear resistance behavior under the temperature above 500 °C. It could be a promising way to improve the high temperature wear resistance by adding NiCr clad $BaF_2{\cdot}CaF_2$ eutectic in $NiCr/Cr_3C_2$ coating.

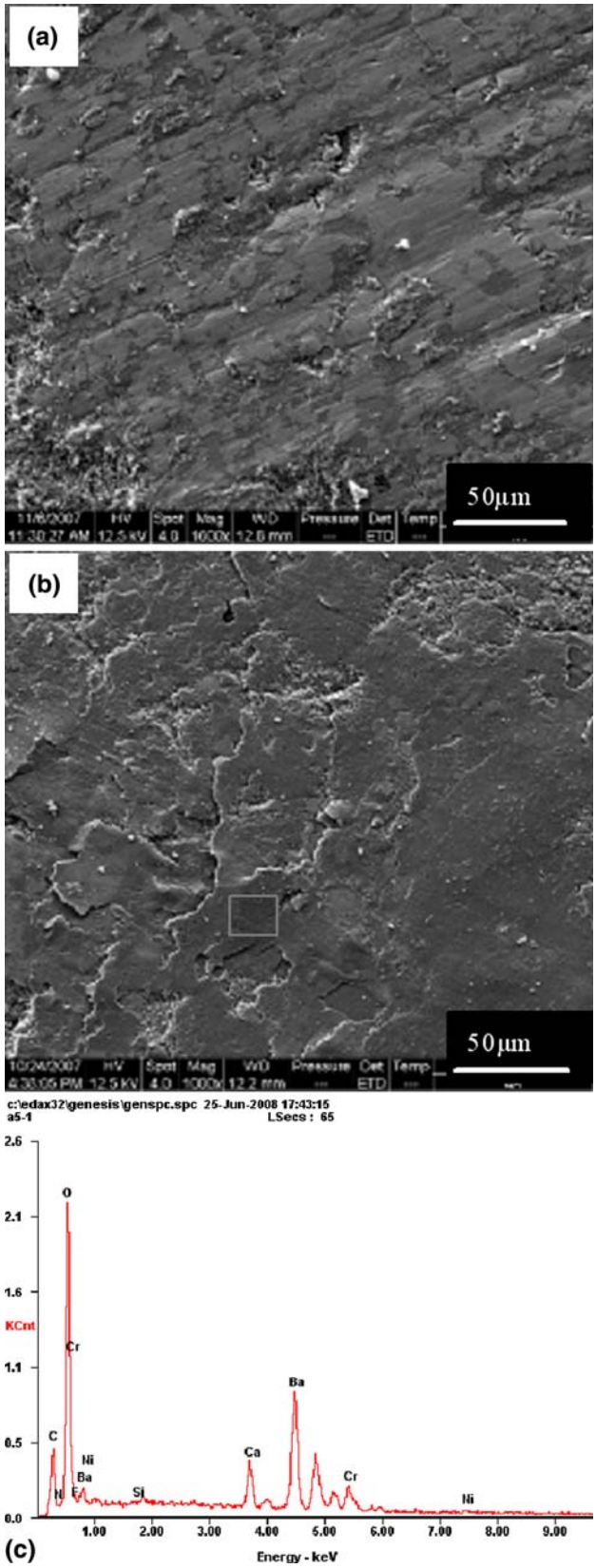

Fig. 7 Worn surfaces of the $NiCr/Cr_3C_2$-10%$BaF_2{\cdot}CaF_2$ coating (a) at room temperature, (b) at 500 °C, and (c) area EDS analysis of (b)

4. Conclusions

(1) NiCr cladding can effectively reduce the difference of density and thermophysical properties between the feedstock components and protect the cores from oxidation and decarburization.

(2) Adding $BaF_2 \cdot CaF_2$ eutectic in the NiCr/Cr_3C_2 feedstock has a negative effect on the mechanical properties of the coating, when the content exceeds 10%, the hardness and bond strength of the coating drop sharply.

(3) $BaF_2 \cdot CaF_2$ eutectic can improve the tribological properties of the NiCr/Cr_3C_2 coating at high temperature. When the temperature reaches higher than 500 °C, the friction coefficient, the wear rates of NiCr/Cr_3C_2-10% $BaF_2 \cdot CaF_2$ coating, and its coupled Si_3N_4 ball are 20%, 40%, and 75% lower than those of the NiCr/Cr_3C_2 coating, respectively.

(4) The dominated wear mechanism of the NiCr/Cr_3C_2-$BaF_2 \cdot CaF_2$ coating at room temperature is splats spallation and abrasive wear, whereas, when the temperature reaches 500 °C, it changes to plastic deformation and plawing by the Si_3N_4 ball.

Acknowledgment

The authors are grateful for the financial support of the National Natural Science Foundation of China (Grant No. 50901071).

References

1. J.M. Guilemany, N. Espallargas, P.H. Suegama, and A.V. Benedetti, Comparative Study of Cr_3C_2-NiCr Coatings Obtained by HVOF and Hard Chromium Coatings, *Corros. Sci.*, 2006, **48**, p 2998-3013
2. G.-C. Ji, C.-J. Li, Y.-Y. Wang, and W.-Y. Li, Microstructural Characterization and Abrasive Wear Performance of HVOF Sprayed Cr_3C_2-NiCr Coating, *Surf. Coat. Technol.*, 2006, **200**, p 6749-6757
3. J.F. Li, L. Li, and C.X. Ding, Thermal Diffusivity of Plasma-Sprayed Cr_3C_2-NiCr Coatings, *Mater. Sci. Eng., A*, 2005, **394**, p 229-237
4. G.-C. Ji, C.-J. Li, Y.-Y. Wang, and W.-Y. Li, Erosion Performance of HVOF-Sprayed Cr_3C_2-NiCr Coatings, *J. Therm. Spray Technol.*, 2007, **16**, p 557-565
5. J.K.N. Murthy, S. Bysakh, K. Gopinath, and B. Venkataraman, Microstructure Dependent Erosion in Cr_3C_2-20(NiCr) Coating Deposited by a Detonation Gun, *Surf. Coat. Technol.*, 2007, **202**, p 1-12
6. S. Matthews, M. Hyland, and B. James, Long-term Carbide Development in High-Velocity Oxygen Fuel/High-Velocity Air Fuel Cr_3C_2-NiCr Coatings Heat Treated at 900 °C, *J. Therm. Spray Technol.*, 2004, **13**, p 526-536
7. H.S. Sidhu, B.S. Sidhu, and S. Prakash, Mechanical and Microstructural Properties of HVOF Sprayed WC-Co and Cr_3C_2-NiCr Coatings on the Boiler Tube Steels Using LPG as the Fuel Gas, *J. Mater. Process. Technol.*, 2006, **171**, p 77-82
8. J.M. Guilemany, N. Espallargas, J. Fernández, P.H. Suegama, and A.V. Benedetti, High-Velocity Oxyfuel Cr_3C_2-NiCr Replacing Hard Chromium Coatings, *J. Therm. Spray Technol.*, 2005, **14**, p 335-341
9. Z. Zhang, X. Lu, and J. Luo, Tribological Properties of Rare Earth Oxide Added Cr_3C_2-NiCr Coatings, *Appl. Surf. Sci.*, 2007, **253**, p 4377-4385
10. C. Dellacorte, Composition Optimization of Chromium Carbide Based Solid Lubricant Coatings for Foil Gas Bearings at Temperatures to 650 °C, NASA TM 179649, 1987
11. H.E. Sliney, Evaluation of PS212 Coatings Under Boundary Lubrication Condition with an Ester-Based Oil to 300 °C, NASA TM106763, 1995
12. G. Kim, H. Choi, C. Han, S. Uhm, and C. Lee, Characterization of Atmospheric Plasma Spray NiCr-Cr_2O_3-Ag-CaF_2/BaF_2 Coatings, *Surf. Coat. Technol.*, 2005, **195**, p 107-115
13. H.E. Sliney, T.N. Storm, and G.P. Allen, Fluoride Solid Lubricants for Extreme Temperature and Corrosive Environments, NASA TM X-52077, 1965
14. Y. Wang and W. Chen, Microstructures, Properties and High-Temperature Carburization Resistances of HVOF Thermal Sprayed NiAl Intermetallic-Based Alloy Coatings, *Surf. Coat. Technol.*, 2004, **183**, p 18-28
15. T. Sundararajan, S. Kuroda, and F. Abe, Steam Oxidation Resistance of Two-Layered Ni-Cr and Al APS Coating for USC Boiler Applications, *Corros. Sci.*, 2005, **47**, p 1129-1147
16. S. Zimmermann and H. Kreye, Chromium Carbide Coatings Produced with Various HVOF Spray Systems, *Thermal Spray: Practical Solutions for Engineering Problems*, C.C. Berndt, Ed., ASM International, Materials Park, Ohio, 1996, p 147-148